Applied Physics Letters

Tunable multimodal magnetoplasmonic metasurfaces

Cite as: Appl. Phys. Lett. **115**, 151102 (2019); https://doi.org/10.1063/1.5124445
Submitted: 15 August 2019 . Accepted: 28 September 2019 . Published Online: 10 October 2019

A. I. Musorin, A. V. Chetvertukhin, T. V. Dolgova, H. Uchida, M. Inoue, B. S. Luk'yanchuk, and A. A. Fedyanin

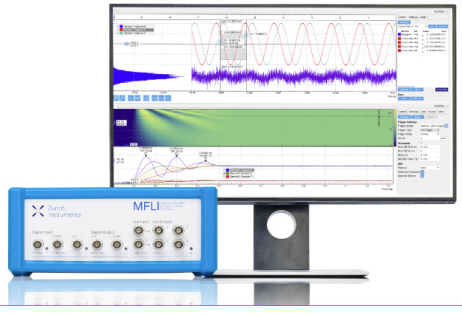

Applied Physics Letters ARTICLE scitation.org/journal/apl

Tunable multimodal magnetoplasmonic metasurfaces

Cite as: Appl. Phys. Lett. **115**, 151102 (2019); doi: 10.1063/1.5124445
Submitted: 15 August 2019 · Accepted: 28 September 2019 ·
Published Online: 10 October 2019

A. I. Musorin,[1] A. V. Chetvertukhin,[1] T. V. Dolgova,[1] H. Uchida,[2] M. Inoue,[2] B. S. Luk'yanchuk,[1,3] and A. A. Fedyanin[1,a)]

AFFILIATIONS

[1]Faculty of Physics, Lomonosov Moscow State University, Moscow 119991, Russia
[2]Department of Electrical and Electronic Information Engineering, Toyohashi University of Technology, 1-1 Tempaku-cho, Toyohashi, Aichi 441-8580, Japan
[3]Division of Physics and Applied Physics, School of Physical and Mathematical Sciences, Nanyang Technological University, Singapore 637371, Singapore

[a)]**E-mail:** fedyanin@nanolab.phys.msu.ru

ABSTRACT

The spectrally controllable enhancement of the transverse magneto-optical Kerr effect is realized in 2D hybrid metal-dielectric magnetoplasmonic metasurfaces. The light diffracted at different interfaces allows one to manipulate light phase in the condition of plasmonic and waveguiding resonance excitation controllable via the azimuthal angle. The multimodal nature of the system provides the flexible tunability of its magneto-optical response.

One of the most rapidly developing areas nowadays is the field of metasurfaces, both metallic[1] and dielectric.[2] These structures are two-dimensional analogs of metamaterials, whose properties are defined by nanostructuring rather than the nature of the materials. The attractive concept of tailoring the optical response for various applications gives rise to the design and development of new metasurface configurations.[3] Plasmonic metasurfaces are known to fully manipulate a phase of light, opening new ways for the creation of flat optical elements such as ultrathin flat lenses,[4] mirrors,[5] polarizers,[6] and wave plates.[7] The dielectric metasurfaces with diffraction elements allow one to bend the light,[8,9] to create a metalens with almost unity numerical aperture.[10] The controllable excitation of Fano-type resonances in plasmonic and all-dielectric metamaterials allows one to govern their optical response and build up new optical,[11] nonlinear-optical,[12,13] and magneto-optical (MO)[14] systems for integrated photonics, solar power,[15] and sensor applications.[16] A specific place among modern photonic research belongs to the idea of topologically protected states.[17] Symmetry breaking plays a crucial role in topological science of spins in solid-state physics and pseudospins in photonics. This permits topologically protected propagation in a forward direction without undesirable backscattering.[18] It is known that the magnetic field breaks time-reversal symmetry. Combining topological photonics with magneto-optics opens the way to nonreciprocal devices driven by a magnetic field. It is expected that a new approach would widen the concept of active metasurfaces controlled by laser pulses[19–21] and electric[22] or magnetic[23] fields.

Numerous magnetophotonic materials and tools were introduced for resonant enhancement of the magneto-optical response based on resonant magnetoplasmons in magnetoplasmonic crystals,[24,25] dielectric cavity modes,[26,27] or Mie-resonant metasurfaces.[28] An increase in the Faraday effect in hybrid metasurfaces can reach one order of magnitude compared with a thin ferromagnetic film.[29] The hybrid metal-dielectric structured materials allow one to improve the magneto-optical figure-of-merit value by reduction of the plasmon losses.[25,30] Nanostructures with magnetic garnets possess a relatively high refractive index and large Faraday rotation, which play a crucial role in photonics application and devices.[31,32] The interaction of local plasmon resonance of a gold nanobar placed on top of a gyrotropic waveguiding layer opens a way to design the magneto-optical nanostructures.[25] Nanoparticles supporting excitation of local plasmon resonances can enhance the magneto-optical signal,[33] for example, nickel nanodisks,[34] core-shell structures with magnetic metal,[35] graphene-based samples,[36] or noble nanospheres incorporated in a magnetic dielectric matrix.[37]

Several orders of diffraction give a possibility for spectral tuning of the optical and magneto-optical response.[38] The manipulation of a magneto-optical signal was recently shown in metallic grating induced by surface plasmon excitation with the variation of the angle of incidence.[24] A few diffraction orders of two-dimensional gold-garnet

nanograting together with the azimuthal angle tuning provide us with the idea of their effective control. For the lattice period of 400 nm and less, only the first diffraction order can be excited at the gold-garnet interface. On the other hand, for a large grating constant, high orders of diffraction are weak, and the diffraction threshold shifts to the infrared. The optimal period of the grating is 600 nm. The next step for the control of the magneto-optical response is the use of two-dimensional gratings. As it was recently shown, the resonant wavelength of surface plasmon excitation can be accurately adjusted in 2D magnetoplasmonic crystals with the azimuthal angle.[39] The additional way of the control is the use of several interfaces between scatters and the environment due to the sensitivity of scatters to it. This gives an advantage compared to the isotropic case when refractive indices under and on top of the lattice are the same,[38] because it allows one to intersect spectrally diffraction orders excited with bottom and top materials.

In this paper, we present a multimodal magnetoplasmonic metasurface with magneto-optical tunability. A dielectric, magnetic matrix with plasmonic inclusions packed in a 2D subwavelength array is designed to manipulate the light by an external magnetic field. The tunability is realized by several interfaces for diffraction (high orders of diffraction) and variation of the azimuthal angle. The experiment shows both plasmonic and high-quality-factor polaritonic magneto-optical resonances tunable by the azimuthal angle. Numerical finite difference time-domain (FDTD) calculations discover the thorough mechanisms of the enhancement. The magneto-optical figure-of-merit value of the device is discussed.

The advantages of internal interface usage can be realized if scatters are placed between media with various refractive indices, e.g., when they are placed on the substrate with refractive index n_1 and covered with a layer with $n_2 > n_1$. If the contrast of refractive indices is high enough, the diffraction maxima on two different interfaces will split spectrally. In this study, the covering layer n_2 is bismuth-substituted yttrium iron garnet (Bi:YIG), $n_2 = n_{Bi:YIG} \approx 2.4$, and substrate n_1 is quartz, $n_1 = 1.45$. In this case, the second diffraction order of n_2 can spectrally overlap the first diffraction order of n_1.

The schematic of the sample and its scanning electron microscopy image are shown in the insets of Fig. 1. The sample is a two-dimensional spatially periodic square lattice of gold nanospheres embedded into a magnetic dielectric layer of Bi:YIG. The periodically ordered gold nanodisks on a silica substrate are fabricated by electron-beam lithography.[37] The array is annealed at 950 °C for 10 min to melt the disks and to form an array of spherical droplets. A dielectric garnet layer is sputtered on top of the array of gold nanospheres by magnetron deposition and annealed at the temperature of 750 °C for crystallization for 15 min. The diameter of the gold nanospheres is 100 nm. The period of the square lattice is 600 nm in both directions. The approximate thickness of the Bi:YIG layer is 100 nm. The surface of the sample has 80-nm hemispheres over spherical gold nanoparticles.

Figure 1 shows magnetic hysteresis loops for a magnetic field applied perpendicular (red curves) and parallel (black curves) to the sample surface. The data are obtained with a vibrating sample magnetometer. A saturation of magnetization in the sample is achieved for an external magnetic field magnitude of 0.75 kOe. In further magneto-optical experiments, an oscillating magnetic field with the saturating amplitude of 1 kOe is applied to the sample.

A conventional setup for transverse magneto-optical Kerr effect (TMOKE) modulation spectroscopy is used in the experiment.[40] A

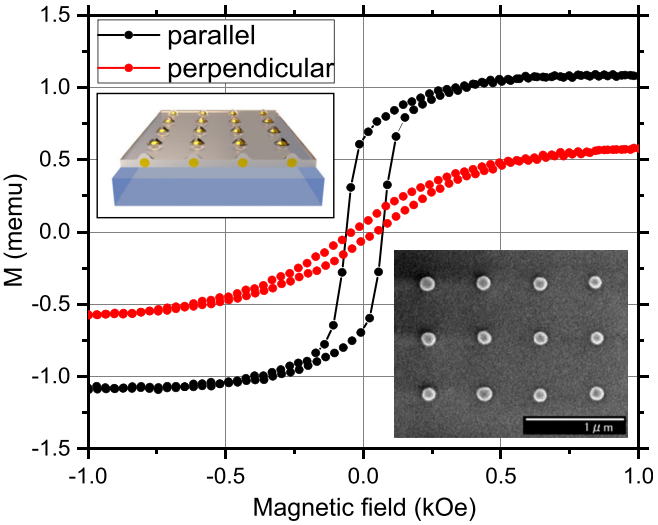

FIG. 1. Vibrating sample magnetometry measurements. The upper inset is a scheme of the sample. The bottom inset is a SEM image of the sample.

radiation source is a polarized light of a halogen lamp. The sample is mounted on a rotation stage, which allows one to change the azimuthal angle with an accuracy of 0.5°. The TMOKE spectra are obtained as follows:[41] $\delta = [T(+H) - T(-H)]/[T(0)]$, where $T(\pm H)$ is the transmittance of the sample for opposite directions of applied external magnetic field H and $T(0)$ is the transmittance without the magnetic field. The light intensity is detected by a photomultiplier tube locked-in to chopper frequency in the case of optical measurements or to the 1-kOe-magnitude magnetic field alternating at 117 Hz in the case of magneto-optical measurements. The MO sensitivity of the experimental setup is $\delta = 3.5 \cdot 10^{-5}$.

Figure 2 shows the experimental (a) and calculated (d) optical transmittance spectra of the magnetoplasmonic metasurface depending on the azimuthal rotation varying from $\varphi = -90°$ to $\varphi = 90°$ for the p-polarized light at the angle of incidence $\theta = 20°$. The azimuthal angle $\varphi = 0°$ set for the tangential component of incoming wave vector $k_{||}$ is parallel to the vector of the reciprocal lattice G [see the inset in Fig. 2(e)]. The results are in good agreement with each other. The color map demonstrates alternating blue (minima) and white (maxima) regions. The sample is designed to support several kinds of resonances. The gold nanoparticles bring a local plasmon resonance in the spectral area of 650 nm. If the phase-matching condition is satisfied, spectrally sharp diffraction peculiarities are overlapped with the wide resonance of local plasmons, leading to the Fano line shape of the resonance. Any resonant feature has a phase change of π over the resonance. When two resonances are hybridized, the total phase change can be 2π. Recently, the hybridization of electric and magnetic dipole Mie resonances in the silicon metasurface allows one to get the transmittance of 100%.[8] In studying magnetoplasmonic metasurfaces when the resonance of the local plasmon is overlapped with Rayleigh anomalies, one can change a minimum of transmittance to a maximum by rotating the sample, i.e., changing the azimuthal angle φ [Fig. 2(a). Compare $\lambda = 725$ nm for $\varphi = 0°$ and $\varphi = 45°$].

The phase-matching condition in 2D lattices, $\mathbf{k}_{||} = \mathbf{k}_d + m_x\mathbf{G}_x + m_y\mathbf{G}_y$, depends not only on an angle of incidence θ and a

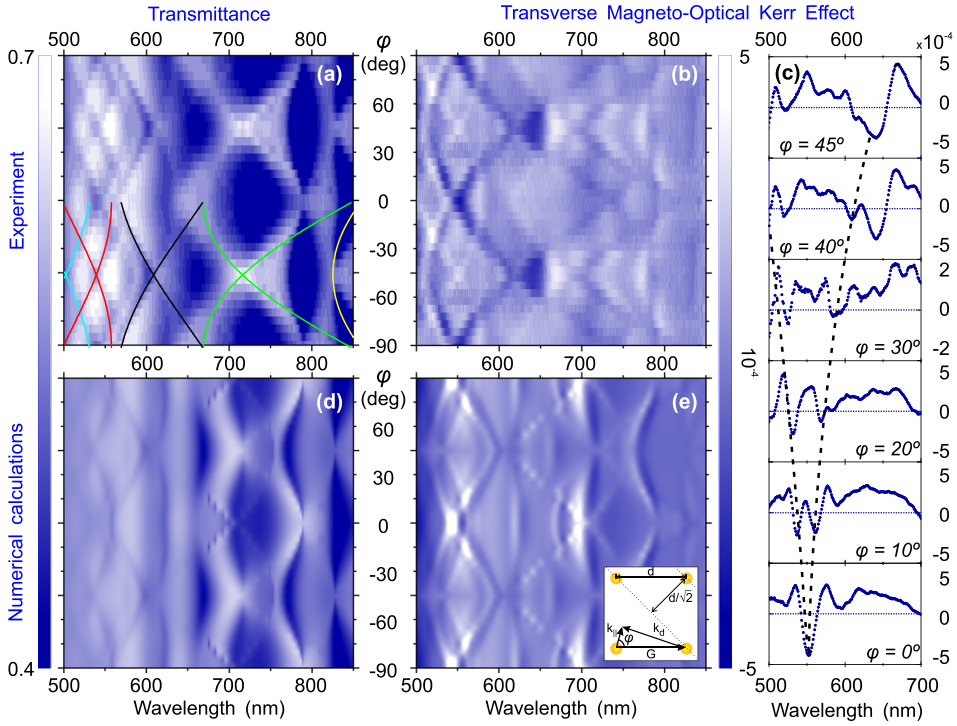

FIG. 2. The experimental (a)–(c) and numerical (d) and (e) azimuthal dependencies of the transmittance (a) and (d) and the magneto-optical (b), (c), and (e) spectra. The color curves on the panel (a) show the Rayleigh anomalies according to Eq. (1): $(0, \pm 1), n_{SiO_2}(\lambda)$ (green); $(0, \pm 1), n_{Bi:YIG}(\lambda)$ (yellow); $(\pm 2, \pm 1), n_{Bi:YIG}(\lambda)$ (black); $(0, \pm 3), n_{Bi:YIG}(\lambda)$ (red); and $(\pm 3, \pm 1), n_{Bi:YIG}(\lambda)$ (cyan). (c) Cross sections of panel (b) through the azimuthal angles (top to bottom): 45°, 40°, 30°, 20°, 10°, 0°. Black dashes curves on the panel (c) are guides to the eye, showing the spectral tuning of the magneto-optical signal. The inset shows a quadratic lattice with the azimuthal angle φ, period d, and $G, k_{||}, k_d$ are a reciprocal lattice vector, tangential component of incoming wave vector, and the wave vector of the diffracted beam.

wavelength λ but also on the azimuthal angle φ. Here, $\mathbf{k}_d$ is a wave vector of diffracted light, m_x and m_y are the diffraction orders, and $\mathbf{G}_x, \mathbf{G}_y$ are the reciprocal vectors in X and Y directions. The diffracted beam propagates along the sample surface, Rayleigh anomaly, for the oblique incidence $\theta \neq 0°$ when the azimuthal angle is consistent with the following condition:

$$\left(\sin\theta\cos\varphi + m_x\frac{\lambda}{nd_x}\right)^2 + \left(\sin\theta\sin\varphi + m_y\frac{\lambda}{nd_y}\right)^2 = 1. \quad (1)$$

Here, d_x and d_y are the lattice periods in X and Y directions and n is a refractive index. In our case, the lattice is quadratic, i.e., $d_x = d_y = d$. These Rayleigh anomalies are shown in Fig. 2(a) by the color curves. The green curve represents the first-order diffraction with $n = n_{SiO_2}$ in Eq. (1). All other dependencies are garnet diffraction, i.e., $n = n_{Bi:YIG}$ in Eq. (1): yellow curve—first order, black—$(\pm 2, \pm 1)$ order, red—third order, and cyan—$(\pm 3, \pm 1)$ order. When the sample is rotated, i.e., when the azimuthal angle φ changes, the spectral positions of Rayleigh anomalies shift. It means that one can tune the optical response of the sample. The fourfold symmetry of the sample's grating leads to transmittance spectra repetition every 90° of the azimuthal angle.

Figure 2(b) shows the experimental spectral dependence of the TMOKE on the azimuthal angle. The brightest peculiarity exists at the wavelength of 650 nm and the azimuthal angle of ±45°. The top panel of Fig. 2(c) shows the cross section of the colormap [Fig. 2(b)] for the angle of $\varphi = 45°$. The magneto-optical feature is the most pronounced, and it has sharp spectral growth and the highest contrast: the switching from the minimum value of $-3 \cdot 10^{-4}$ of the effect to the maximum one of $4 \cdot 10^{-4}$. This value is one order of magnitude higher than that of off-resonant spectral regions of the structure or a flat Bi:YIG film, where δ equals $4 \cdot 10^{-5}$. This peculiarity is associated with the excitation of quadrupole plasmon resonance in gold nanoparticles. To estimate the magneto-optical figure-of-merit, we define an efficiency value as $\eta = T \cdot |\delta|/h = 0.28\ \%/\mu\text{m}$, where T is the transmittance, δ is the TMOKE, and h is the thickness of the structure. The pattern of local fields, typical for this resonance (clover-structured), explains the brightness of the TMOKE in the vicinity of 45°. The light effectively concentrates at the gold particle–magnetic dielectric interface. This radiation localization enhances the magneto-optical response. A change of a sign of the effect occurs within only 20 nm, i.e., it is a very narrow feature. This feature can be promising for ultrafast magneto-optical switching[19,42] or the femtosecond pulse modulation by an external magnetic field.[43,44]

The dip in the TMOKE spectra is shifted toward UV wavelengths with the azimuthal sample rotating away from $\varphi = 45°$. The effect reaches the value of $-4 \cdot 10^{-4}$ at a wavelength of $\lambda \approx 550$ nm, when a waveguiding mode is excited. This spectral tuning of the magneto-optical resonance is the evidence of the opportunity for accurate manipulation of light intensity by the external magnetic field. To verify experimental data, numerical simulations are carried out with the commercial software Lumerical FDTD Solutions. The Maxwell equations are solved using the finite difference time-domain method adapted to perform magneto-optical simulations. A single cell of the structure is modeled with periodic boundary conditions in X and Y directions (period 600 nm) and perfectly matched layers in the Z direction. A plane wave source with a broadband spectrum (475–975 nm) illuminates the lattice unit cell under the 20° angle of incidence. The plane of incidence is the xOz plane (see the inset in Fig. 3). The polarization belongs to this plane, which corresponds to the P-polarized

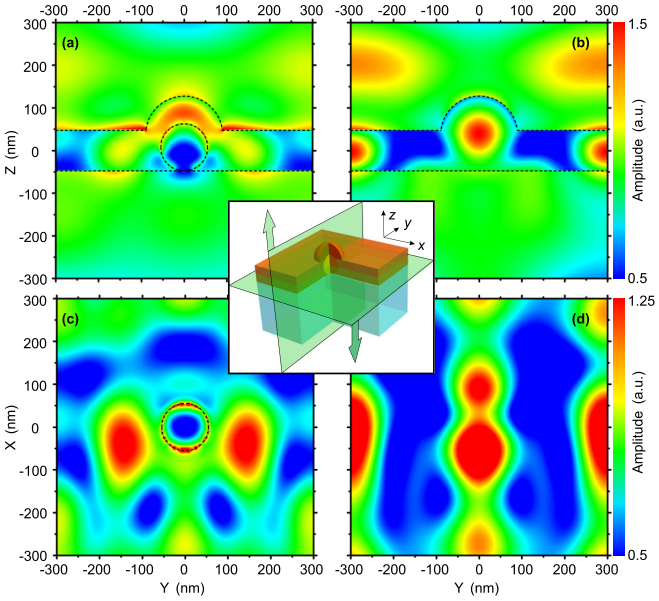

FIG. 3. Calculated field distribution $|Re(E_x)|$. (a) and (b) are side views and (c) and (d) are top views of the structure in the case of the existence (a) and (c) and absence (b) and (d) of gold nanospheres. The inset in the middle is a sketch of an elementary cell of the sample.

light. The external magnetic field is parallel to the Y-axis. The transmittance spectra were calculated using grating transmission analysis, which allows one to reproduce completely the experimental conditions, where only zero order of diffraction is detected.

A gold sphere with a radius of 55 nm is placed on a bulk quartz substrate and inside a 95-nm-thick Bi:YIG film. The Bi:YIG hemisphere of 80-nm radius is positioned above the gold sphere to reproduce the topology of the experimental sample according to the atomic-force-microscopy data. A mesh step around the gold nanoparticle was decreased down to 5 nm. The dispersion of optical constants of the materials and a magneto-optical constant of Bi:YIG are taken into account.[45–47]

Numerical simulation repeats the features observed in transmittance [compare Figs. 2(a) and 2(d)] and TMOKE (compare Figs. 2(b) and 2(e)] spectra. To understand the nature of the dip near the wavelength of 550 nm in the case of $\varphi = 0°$ [Fig. 2(c), bottom panel], the local electric field distribution of the light wave is calculated. Figure 3 shows a distribution of the magnitude of the real part of the X-component of the electric field. The wavelength corresponds to the dip around 550 nm in the transmittance spectrum. Figure 3(a) shows the YZ cross section and (c) shows the YX cross section through the middle of the spherical particle, i.e., side and top views (see the insets in Fig. 3). The field strongly concentrates in Bi:YIG bulbs and near the Bi:YIG-air interface. This spectral peculiarity is strongly related to the existence of these bulbs over gold nanospheres. To check this idea, the simulation is repeated without Au nanoparticles [see Fig. 3(b): side view and (d): top view]. The transmittance spectrum shows a similar dip at the wavelength around 550 nm, while in the case of a flat Bi:YIG film, without bulbs, the dip disappears. The distribution of the electric field in a side view [see Fig. 3(b)] shows a periodic pattern, which is induced by the Bi:YIG hemispheres. It means that garnet bulbs scatter incoming light and form a standing wave inside the garnet layer. These bulbs can be considered as a phase grating because these scatters are dielectric opposite to gold nanospheres which form an amplitude grating. Thus, there is a mode in this spectral area, which is excited by periodically arranged hemispheres of Bi:YIG, i.e., at the Bi:YIG-air interface. This is another reason for the explanation of the enhancement of the magneto-optical signal in this spectral region [Fig. 2(c), bottom panel].

In conclusion, accurate tuning of the transverse magneto-optical Kerr effect is experimentally demonstrated and numerically supported in hybrid metal-dielectric magnetoplasmonic metasurfaces based on a thin magnetic garnet film with a two-dimensional gold nanograting inside. Spectral tuning of magneto-optical resonances with a variation of the azimuthal angle is the evidence of the possibility for light intensity manipulation via applying an external magnetic field. The efficiency of the magnetoplasmonic metasurface reaches the value of $\eta = 0.28\ \%/\mu m$ for the angle of incidence $\theta = 20°$. The TMOKE is an angle-of-incidence-dependent effect, and for large angles, the value of η should be greater.[41] The other way for making the sample more efficient is increasing the Bi concentration in the garnet film (0.3 in the study).[41] A promising way to enlarge the effect is changing absorbing gold nanoparticles with high refractive index analogs, like silicon,[2] or core-shell structures.[35] Magnetoplasmonic crystals, similar magneto-optical systems but forced with surface plasmon-polaritons, in transmission mode demonstrate $\eta = 0.012\%/\mu m$,[25] which is more than 20 times smaller than that for magnetoplasmonic metasurfaces. Magnetoplasmonic crystals reach high TMOKE parameter δ due to quite thick gyrotropic material ($h = 2.5\ \mu m$), but transmittance is only 2% because of wide gold strips covering the garnet layer that possess a significant imaginary part of the dielectric constant. It has been shown[48] that similar periodic structures in the microwave domain can be implemented to realize topologically protected states by introducing bianisotropy to the system. However, magnetic permeability at optical frequencies is unity, and bianisotropy is hard to achieve. However, it is possible to tune their effective values in the vicinity of electric and magnetic dipole resonances. They can be reached in nonabsorbing nanoparticles with a high refractive index or in plasmonic split-ring resonators. We believe that magnetoplasmonic metasurfaces can be optimized for topological photonic devices controllable by a magnetic field if one replaces the gold nanospheres with particles with electric and magnetic dipole resonances.

The authors thank N.S. Perov for the vibrating sample magnetometer experiments. This work was supported by the Japan Society for the Promotion of Science (JSPS) and the Ministry of Science and Higher Education of the Russian Federation (Grant N14. W03.31.0008, sample fabrication). The experimental part of work is supported by the Russian Science Foundation (No. #19-72-00168). The numerical calculations are made with the support of the Russian Foundation for Basic Research (Nos. #17-52-560011 and #18-52-50021). The research was partly supported by the MSU Quantum Technology Center.

REFERENCES

[1]N. Yu and F. Capasso, Nat. Mater. **13**, 139 (2014).
[2]A. I. Kuznetsov, A. E. Miroshnichenko, M. L. Brongersma, Y. S. Kivshar, and B. Luk'yanchuk, Science **354**, aag2472 (2016).

[3]A. Y. Zhu, A. I. Kuznetsov, B. Luk'yanchuk, N. Engheta, and P. Genevet, Nanophotonics **6**, 452 (2017).
[4]F. Aieta, P. Genevet, M. A. Kats, N. Yu, R. Blanchard, Z. Gaburro, and F. Capasso, Nano Lett. **12**, 4932 (2012).
[5]A. Pors, M. G. Nielsen, R. Eriksen, and S. I. Bozhevolnyi, Nano Lett. **13**, 829 (2013).
[6]Y. Zhao, M. Belkin, and A. Alù, Nat. Commun. **3**, 870 (2012).
[7]N. Yu, F. Aieta, P. Genevet, M. A. Kats, Z. Gaburro, and F. Capasso, Nano Lett. **12**, 6328 (2012).
[8]Y. Yu, A. Y. Zhu, R. Paniagua-Domínguez, Y. Fu, B. Luk'yanchuk, and A. I. Kuznetsov, Laser Photonics Rev. **9**, 412 (2015).
[9]E. Khaidarov, H. Hao, R. Paniagua-Domínguez, Y. Yu, Y. Fu, V. Valuckas, S. Yap, Y. T. Toh, J. Ng, and A. Kuznetsov, Nano Lett. **17**, 6267 (2017).
[10]R. Paniagua-Dominguez, Y. Yu, E. Khaidarov, S. Choi, V. Leong, R. M. Bakker, X. Liang, Y. H. Fu, V. Valuckas, L. Krivitsky, and A. Kuznetsov, Nano Lett. **18**, 2124 (2018).
[11]R. Guo, E. Rusak, I. Staude, J. Dominguez, M. Decker, C. Rockstuhl, I. Brener, D. N. Neshev, and Y. S. Kivshar, ACS Photonics **3**, 349 (2016).
[12]J. Reinhold, M. R. Shcherbakov, A. Chipouline, V. I. Panov, C. Helgert, T. Paul, C. Rockstuhl, F. Lederer, E.-B. Kley, A. Tünnermann *et al.*, Phys. Rev. B **86**, 115401 (2012).
[13]L. Wang, A. S. Shorokhov, P. N. Melentiev, S. Kruk, M. Decker, C. Helgert, F. Setzpfandt, A. A. Fedyanin, Y. S. Kivshar, and D. N. Neshev, ACS Photonics **3**, 1494 (2016).
[14]M. N. Romodina, I. V. Soboleva, A. I. Musorin, Y. Nakamura, M. Inoue, and A. A. Fedyanin, Phys. Rev. B **96**, 081401 (2017).
[15]Y. Wang, T. Sun, T. Paudel, Y. Zhang, Z. Ren, and K. Kempa, Nano Lett. **12**, 440 (2012).
[16]W. Withayachumnankul, K. Jaruwongrungsee, A. Tuantranont, C. Fumeaux, and D. Abbott, Sens. Actuators, A **189**, 233 (2013).
[17]D. Dobrykh, A. Yulin, A. Slobozhanyuk, A. Poddubny, and Y. S. Kivshar, Phys. Rev. Lett. **121**, 163901 (2018).
[18]A. P. Slobozhanyuk, A. B. Khanikaev, D. S. Filonov, D. A. Smirnova, A. E. Miroshnichenko, and Y. S. Kivshar, Sci. Rep. **6**, 22270 (2016).
[19]C. D. Stanciu, F. Hansteen, A. V. Kimel, A. Kirilyuk, A. Tsukamoto, A. Itoh, and T. Rasing, Phys. Rev. Lett. **99**, 047601 (2007).
[20]A. S. Shorokhov, K. I. Okhlopkov, J. Reinhold, C. Helgert, M. R. Shcherbakov, T. Pertsch, and A. A. Fedyanin, Sci. Rep. **6**, 28440 (2016).
[21]M. R. Shcherbakov, S. Liu, V. V. Zubyuk, A. Vaskin, P. P. Vabishchevich, G. Keeler, T. Pertsch, T. V. Dolgova, I. Staude, I. Brener *et al.*, Nat. Commun. **8**, 17 (2017).
[22]P. P. Iyer, M. Pendharkar, and J. A. Schuller, Adv. Opt. Mater. **4**, 1582 (2016).
[23]M. G. Barsukova, A. S. Shorokhov, A. I. Musorin, D. N. Neshev, Y. S. Kivshar, and A. A. Fedyanin, ACS Photonics **4**, 2390 (2017).
[24]A. A. Grunin, A. G. Zhdanov, A. A. Ezhov, E. A. Ganshina, and A. A. Fedyanin, Appl. Phys. Lett. **97**, 261908 (2010).
[25]J. Y. Chin, T. Steinle, T. Wehlus, D. Dregely, T. Weiss, V. Belotelov, B. Stritzker, and H. Giessen, Nat. Commun. **4**, 1599 (2013).
[26]A. A. Fedyanin, T. Yoshida, K. Nishimura, G. Marowsky, M. Inoue, and O. A. Aktsipetrov, J. Magn. Magn. Mater. **258–259**, 96 (2003).
[27]S. Kahl and A. Grishin, Appl. Phys. Lett. **84**, 1438 (2004).
[28]A. I. Musorin, M. G. Barsukova, A. S. Shorokhov, B. S. Luk'yanchuk, and A. A. Fedyanin, J. Magn. Magn. Mater. **459**, 165 (2018).
[29]M. G. Barsukova, A. I. Musorin, A. S. Shorokhov, and A. A. Fedyanin, APL Photonics **4**, 016102 (2019).
[30]E. Almpanis, P. Pantazopoulos, N. Papanikolaou, V. Yannopapas, and N. Stefanou, J. Opt. Soc. Am. B **33**, 2609 (2016).
[31]K. Takahashi, F. Kawanishi, S. Mito, H. Takagi, K. Shin, J. Kim, P. Lim, H. Uchida, and M. Inoue, J. Appl. Phys. **103**, 07B331 (2008).
[32]Y. Shoji, T. Mizumoto, H. Yokoi, I.-W. Hsieh, and R. M. Osgood, Jr., Appl. Phys. Lett. **92**, 071117 (2008).
[33]I. Maksymov, Rev. Phys. **1**, 36 (2016).
[34]V. Bonanni, S. Bonetti, T. Pakizeh, Z. Pirzadeh, J. Chen, J. Nogués, P. Vavassori, R. Hillenbrand, J. Åkerman, and A. Dmitriev, Nano Lett. **11**, 5333 (2011).
[35]L. Wang, C. Clavero, Z. Huba, K. J. Carroll, E. E. Carpenter, D. Gu, and R. A. Lukaszew, Nano Lett. **11**, 1237 (2011).
[36]D. Kuzmin, I. Bychkov, V. Shavrov, and V. Temnov, Nanophotonics **7**, 597 (2018).
[37]H. Uchida, Y. Mizutani, Y. Nakai, A. A. Fedyanin, and M. Inoue, J. Phys. D **44**, 064014 (2011).
[38]M. Kataja, T. Hakala, A. Julku, M. Huttunen, S. van Dijken, and P. Törmä, Nat. Commun. **6**, 7072 (2015).
[39]A. A. Grunin, N. A. Sapoletova, K. S. Napolskii, A. A. Eliseev, and A. A. Fedyanin, J. Appl. Phys. **111**, 07A948 (2012).
[40]A. A. Grunin, I. R. Mukha, A. V. Chetvertukhin, and A. A. Fedyanin, J. Magn. Magn. Mater. **415**, 72 (2016).
[41]A. K. Zvezdin and V. A. Kotov, *Modern Magnetooptics and Magnetooptical Materials* (CRC Press, 1997).
[42]E. Beaurepaire, G. Turner, S. Harrel, M. Beard, J.-Y. Bigot, and C. Schmuttenmaer, Appl. Phys. Lett. **84**, 3465 (2004).
[43]M. R. Shcherbakov, P. P. Vabishchevich, A. Y. Frolov, T. V. Dolgova, and A. A. Fedyanin, Phys. Rev. B **90**, 201405 (2014).
[44]A. I. Musorin, M. I. Sharipova, T. V. Dolgova, M. Inoue, and A. A. Fedyanin, Phys. Rev. Appl. **6**, 024012 (2016).
[45]P. Hansen and J.-P. Krumme, Thin Solid Films **114**, 69 (1984).
[46]P. B. Johnson and R. W. Christy, Phys. Rev. B **6**, 4370 (1972).
[47]E. D. Palik, *Handbook of Optical Constants of Solids*, Vol. 3 (Academic Press, 1998).
[48]X. Ni, D. Purtseladze, D. A. Smirnova, A. Slobozhanyuk, A. Alù, and A. B. Khanikaev, Sci. Adv. **4**, eaap8802 (2018).